Optimization of ZnSnO/CIGS Solar Cell with the Incorporation of Cu_2O-EBL Layer

Alisha Priya[1], Prashant Kumar[2], Shiva Nand Singh[3]

Department of Electronics & Communication Engineering

NIT Jamshedpur, India

E-mail:- *2019rsec004@nitjsr.ac.in[1], prashant.ece@nitjsr.ac.in[2], snsingh.ece@nitjsr.ac.in[3]*

DOI: - https://doi.org/10.47531/MANTECH/ECC.2021.54

Abstract

In this article, the study of CIGS solar cells is carried out by employing 1-dimensional numerical simulations using the simulator AFORS-HET. Here simulation of the conventional structure of Al/SLG/ZnO: Al/i-ZnO/ZnSnO/CIGS/Mo solar cell is done in which experimental values are used for the verification of the simulation. Also, a novel architecture is designed by incorporating the cuprous oxide (p-type Cu2O) layer as an electron blocking layer (EBL)at back-contact for the reduction of the minority carrier recombination loss. The parameters of the cell are optimized at different concentrations of doping and thickness to get better performance. The obtained efficiency of the proposed structure is raised by 9.62% in comparison to the experimental work.

Keywords: - *Cu_2O, CIGS, EBL, BSF, CBD*

.

INTRODUCTION

$CuIn_{1-x}Ga_xSe_2$ (CIGS) based thin-film solar cells are considered more compared to others because of its relatively low-cost property along with its higher efficiency. In the most recent research, on an experimental scale, the thin-film based CIGS solar cells have proven with conversion efficiency (η) of 23.82% [1], and on the simulation scale, it's 27.48% [2]. Commonly there are five layers in a CIGS solar cell structure. The first step in the manufacturing of this structure is the deposition of the back contact molybdenum (Mo) layer. Usually, this deposition is carried out by DC magnetron sputtering, used on metallic foil or clean soda-lime glass. After this, the deposition of the p-type CIGS absorber layer is completed. Co-evaporation, salinization/sulfurization of metallic precursors are few technologies that are used for this. When the CIGS reacted with Mo layers creates the $MoSe_2$ layer, which provides the quasi-ohmic contact between the absorber and the Mo back contact [3]. After this, with chemical bath deposition (CBD), the CdS layer of n-type is developed. For avoiding the direct connection between the transparent conductive oxide (TCO) layer with CIGS, especially for those areas which are not changed enough by CdS, an intrinsic ZnO layer deposit. A less-resistive and more-thick ZnO: Al deposited on the i-ZnO layer as the TCO.

In recent investigations, researchers are more attracted to the conversion and optimization of the structure. This includes works like multi-layer wideband anti-reflection coating, utilization of a cover glass integrated with sub-wavelength designs, and for enhancing the spectral response of the cell usage of quantum dots [4]. Also, it includes the usage of deposition using the atomic layer deposition method for the preparation of complete CIGS solar cells, flexible fabrication cells at low- temperature processes, analysis of the substrate temperature effect on the performance of cells[5], and also the alkali treatments of these solar cells.

In the fabrication of CIGS based solar cells, the most common material used for buffer layers is CdS. On the other hand, the harmful nature of Cd makes the usage of CdS unfavourable, the participation of a non-vacuum chemical bath deposition (CBD) method, and lower energy of bandgap (~2.4 eV), photons of higher-energy in the 330 to 350 nm range of the sunlight spectrum are prevented by these reasons from arriving in the CIGS[6]. There are some good electrical properties given by the CdS buffer. Hence, CIGS based solar cell does not provide suitable conduction bands arrangement, which leads to depletion in their performances. Therefore, it is essential to obtain the right p-n junction that a

buffer layer that consists of an appropriate lattice parameter and band offset is adequately matched to the CIGS absorber layer [7].

Much research has been carried out to get a more suitable replacement for Cd free buffer layers. Nowadays, there are more research interests in areas where the substitute of Cd-free buffer material for CIGS solar cells, $Zn_{1-y}Sn_yO$ (ZnSnO), is used[8]. It's the sizeable tunable bandgap with various levels of Sn content, having abundant constituent elements, and its excellent stability are the advantages of ZnSnO film.

In the 80s, much exciting work is done related to the back surface field (BSF) layer, and it's an effect that it carries on the cell efficiency [9]. For repelling the carriers at the CIGS/BSF heterojunction, an extensive bandgap material is used as a barrier specifically for reducing the losses in carriers at the back contact. Along with it, it decreases the back contact carrier recombination and hence improves the efficiency of the cell. There are several studies carried out related to the use of the electron blocking layer (EBL) since it can play the same character as the BSF layer. It can also help in promoting the performance of the cell. Cuprous oxide (Cu_2O), which has a wide bandgap in a range from 2.1 to 2.61 eV and p-type conductivity, is one of the promising materials which can be used as an EBL layer [10]. Cu_2O is an inexpensive, right away available, non-toxic material. In a visible range, it's absorption coefficient is large, which makes it an even more rising material for usage [11].

In this proposed work, mathematical simulation of thin-film based CIGS solar cells is done with the help of the AFORS-HET simulation tool software. Here simulated results and the electrical parameters are validated with the experimental conventional solar cell structure, as reported in [12]. After the simulation of traditional architecture, almost similar results are obtained between the simulated and experimental architectures. Also, a new model proposed in which Cu_2O is incorporated as an EBL layer in CIGS solar cells for improving cell performance. Here, we studied the effects of the doping concentration, energy bandgap, and thickness of CIGS and Cu_2O as an EBL layer.

DEVICE STRUCTURE MODELING, SIMULATION AND MATERIALS PROPERTIES

AFORS-HET is a good simulator due to its accurate results. Here, AFORS-HET is used for designing and optimizing the structure of CIGS solar cells. There are several models on which the calculations are dependent, which is somehow depend on some mathematical relations. Like, the continuity equations and carrier transport in which densities of electron and hole is obtained to establish the effect of transport, generation, and recombination processes [13]. The mobility model is useful in the study of ZnSnO/CIGS solar cells in which holes and electrons moved in a field that is doped. There are two models used for recombination, the Shockley- Read-Hall (SRH) and radiative recombination. At the thermal equilibrium, the Fermi-Dirac stats are useful to define the behavior of the carriers.

First, the simulation of the reference cell is done [12]. Fig. 1 represents the schematic representation of the architecture. It consists of the n-ZnSnO/p-CIGS heterojunction having a concentration of doping are $1x10^{20}$ cm^{-3} and $1.5x10^{16}$ cm^{-3}, respectively. The layer of zinc oxide, which is aluminium doped, is used to form the front contact as a window layer. The HRT layer, which is developed by using undoped ZnO, is put in between the ZnSnO buffer layer and a front-contact window layer. Also, 10 nm/10 nm of (Al/Ni) is used to model the front-contact metal layer. Similarly, Mo is used as a back contact metal layer.

Table I shows the list of the parameters used in the simulation of the architecture of the cell. 0.25 cm^2 of the area is preferred for this device. For simulation purpose, 300 K of operating temperature and incident irradiation of 1000 W/m^2 is used.

Fig. 1 represents the characteristics curve of current density and voltage (J-V) of the simulated solar cell discussed in[12]. An acceptable result is obtained for both curves that show the parameters used as inputs are selected in the simulation is justifiable.

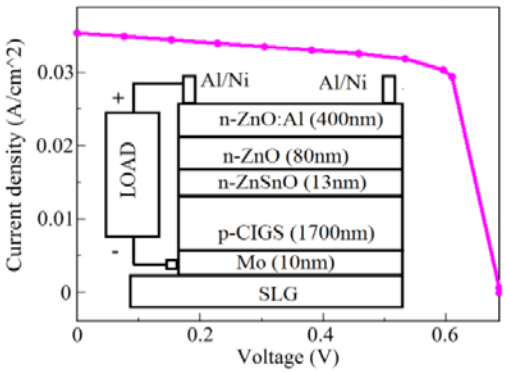

Fig. 1: Schematic representation of ZnSnO/CIGS heterojunction conventional solar cell

Table II shows the experimental and simulation results of the solar cell derived from Fig. 1. The almost fair settlement between the results obtained by either simulation or by experiment. This establishes that the specification used in simulation and the respective architecture is appropriate.

In order to maximize the carrier recombination and improve cell performance, Cu_2O EBL thin layer is inserted in the middle of the back contact and the absorber layer.

Fig. 2 explains the schematic structure of the proposed Al/ZnO:

Al/ZnO/ZnSnO/CIGS/Cu_2O/Mo/SLG solar cell architecture. Table I shows the lists of the parameters of the proposed structure layer material.

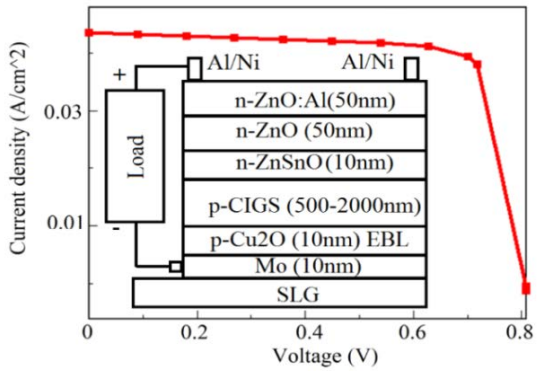

Fig. 2: Schematic representation of ZnSnO/CIGS heterojunction Proposed solar cell

A. Simulation Platform

In this paper, a mathematical computer package for simulation of heterojunction solar cells known as Automat (AFORS-HET version 2.5) software tool is used. The one- dimensional numerical analysis simulator tool built-up Helmholtz-Zentrum Berlin fur Materialien and Energie institute of berlin, Germany [13].

AFORS-HET is a powerful, dominant device simulation software tool. That is why it is capable of simulating both AC as well as DC measurement of electrical and optical specifications of the devices of the solar cells. The AFORS-HET software is also qualified for solving the basic semiconductor equations such as the Poisson equation, related to the electric field displacement, and current density continuity equations for electrons and holes. The following expressions obtained from the article:

The relation of Poisson and continuity equation are discussed below by (1) – (3):

$$\frac{\partial D}{\partial x} = +q\left(p - n + N_d^+ - N_a^- + \frac{\rho_{def}}{q}\right) \quad (1)$$

$$\frac{\partial J_n}{\partial x} = -q(G - R_n) \quad (2)$$

$$\frac{\partial J_p}{\partial x} = +q(G - R_p) \quad (3)$$

Where D is the displacement, n and p are electron and hole densities, ρ_{def} is defect charge density, $N_{d/a}$ is donor and acceptor concentration, respectively, $J_{n/p}$ are electron and hole current, and G is the optical generation rate. The notation of R_n and R_p shows the net recombination rate of electrons and holes.

B. Electrical Parameter of Respective Materials

The electrical and optical properties of the material of all the layers are input to the AFORS-HET simulator program. Table I summarizes the material properties of all layers [14-19]. In this structure, the tuning of acceptor density and thickness of the CIGS absorber layer is between $1x10^{16}$ - $1x10^{17}cm^{-3}$ and 500-2000nm, respectively.

For simulation, the main parameters required include the width of the layer, energy bandgap (E_g), electron affinity (χ), dielectric constant ($\varepsilon/\varepsilon_0$), the state density conduction band (N_c), the state density valance band (N_v), electron thermal velocity (V_e), hole thermal velocity (V_h), electron mobility (μ_e), hole mobility (μ_h), capture cross-section for electro (σ_e), capture cross-section for the hole (σ_h), and total defect density (N_t).

RESULTS AND DISCUSSION

A. Effects of the VOC, JSC, FF, and % η due to change of CIGS thickness and acceptor doping concentration

Fig. 3 displays that when the thickness of the CIGS layer rises from 500 to 2000nm, the JSC, VOC, and efficiency rise quickly, and the value of the fill factor decline. The fill factor FF continues to fall when the thickness is beyond 1500nm, and all the other parameters are almost constant.

Table I: Data values used in the simulation

Parameters	ZnO:Al	ZnO	ZnSnO	CIGS	Cu_2O
E_g (eV)	3.287	3.3	3.7	1.265	2.1
χ (eV)	4.55	4.3	4.7	4.7	4.1
$\varepsilon/\varepsilon_0$	9	8.12	8	13.6	9

N_c (cm^{-3})	$3x10^{18}$	$1x10^{18}$	$1.2x10^{18}$	$2x10^{18}$	$1.3x10^{18}$
N_v (cm^{-3})	$1.8x10^{19}$	$1.8x10^{19}$	$1.8x10^{19}$	$1.5x10^{19}$	$2.4x10^{19}$
V_e($cm\ s^{-1}$)	$2.4x10^{7}$	$3x10^{5}$	$2.4x10^{7}$	$3.9x10^{7}$	$1x10^{7}$
V_h($cm\ s^{-1}$)	$1.3x10^{7}$	$1.5x10^{5}$	$1.3x10^{7}$	$1.4x10^{7}$	$1x10^{7}$
μ_e($cm^2\ V^{-1}s^{-1}$)	100	100	100	100	100
μ_h($cm^2\ V^{-1}s^{-1}$)	10	10	31	25	25
Nd(cm^{-3})	$1x10^{18}$	$1x10^{20}$	$1x10^{19}$	0	0
Na(cm^{-3})	0	0	0	$1.5x10^{16}$	$1x10^{16}$
Auger coefficient electron (cm^6/s)	$1.12x10^{13}$	$1.12x10^{13}$	$1.12x10^{13}$	$1x10^{-28}$	$3x10^{-27}$
Auger coefficient hole (cm^6/s)	$1.12x10^{13}$	$1.12x10^{13}$	$1.12x10^{13}$	$1x10^{-28}$	$2x10^{-27}$
Band to band recombination coefficient (cm^3/s)	$1.2x10^{-12}$	$1.2x10^{-12}$	$1.2x10^{-12}$	$8x10^{-11}$	$9x10^{-15}$
σ_e (cm^2)	$1x10^{-15}$	$3x10^{-15}$	$1x10^{-15}$	$1x10^{-15}$	$1x10^{-14}$
σ_h(cm^2)	$1x10^{-12}$	$3x10^{-14}$	$5x10^{-13}$	$5x10^{-13}$	$1x10^{-14}$
N_t (cm^{-3})	$1x10^{16}$	$5.6x10^{18}$	$1x10^{13}$	$1x10^{14}$	$1x10^{14}$

Table II: Experimental and simulation electrical parameters of conventional ZnSnO/CIGS solar cell

Parameters	Experimental result	Simulation result
V_{OC} (mV)	684	686
J_{SC} (mA/cm^2)	35.2	35.31
FF (%)	74.9	75.55
η (%)	18	18.06

Also, as the thickness of the absorber layer increased, the photons absorbing rate of the CIGS layer raise. More number of electron-hole pairs are generated by the absorption of photons. Due to which photo-current Iph rises, and hence the performance of electrical parameters of ZnSnO/CIGS heterojunction thin-film solar cell (HTFSC) is increased.

The acceptor doping density of the CIGS layer increased from $1x10^{16}$ to $1x10^{17}cm^{-3}$, the V_{OC}, FF, and efficiency increase rapidly, and then it remains constants. The V_{OC} has increased due to a decrease in the photogenerated reverse saturation current density J_{SC}.

However, the J_{SC} slightly decreased due to an increase in acceptor doping density. The depletion region width depletes due to the rise of the doping density of the acceptor. That's why J_{SC} will slightly reduce [2]. Moreover, the doping density of the CIGS acceptor increases from $1x10^{16}$ to $1x10^{17}cm^{-3}$, and hence efficiency increases. The efficiency decreases at the above of $1.5x10^{16}$ cm^{-3} doping density. The efficiency attains a peak value of 27.62% at $1.5x10^{16}cm^{-3}$ and 1500nm, which is the optimal doping density of CIGS and thickness

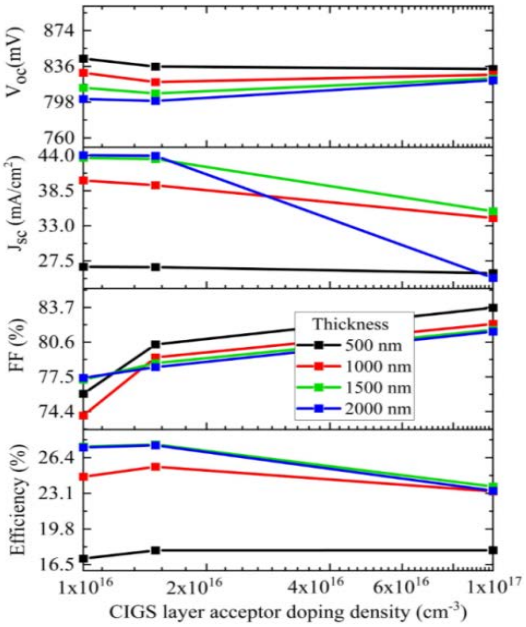

Fig. 3: Impact of electrical parameters with the variation of acceptor density and thickness of the absorber layer of CIGS

B. Effect of EQE CIGS absorber layer at distinct thicknesses

The absorber layer of CIGS thickness varies from 500nm to 2500nm, then the EQE of proposed solar cells also varies at this time. All other cell parameters are kept constant.

Fig. 4 shows the performance of EQE versus wavelength at different thicknesses of the absorber layer of CIGS. When the thickness of the absorber layer increases from 500 to 2500nm, then the photogenerated minority carrier (i.e., electrons) recombination loss also increases in the CIGS absorber layer region. Therefore both JSC and EQE are decreased.

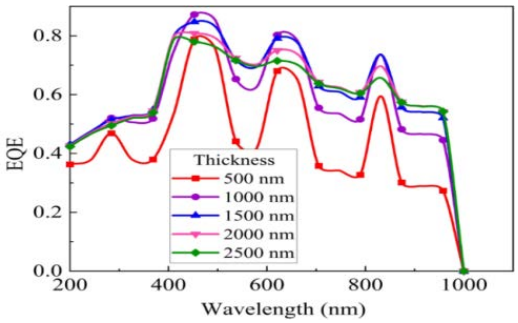

Fig. 4: Wavelength- EQE with different thickness of the CIGS absorber layer.

C. Impact of different Energy bandgap of Cu_2O as an EBL of a ZnSnO/CIGS Solar Cell

The performance of electrical parameters increases when the energy band gap of p-Cu_2O as EBL increases, which is shown in table III. Keeping all other layer parameters of the proposed cell is constant. When the energy band gap of p-Cu_2O as an EBL is less than and higher than 2.1eV, the performance of J_{SC}, FF, $V_{OC,}$ and efficiency get decreased due to the presence of minority carrier recombination (i.e., electrons) of the p-type region. However, beyond the 2.1eV energy bandgap of p-Cu_2O as an EBL, the performance V_{OC}, J_{SC}, FF, and efficiency reach the maximum values.

Table III: Varation of energy bangap of cu2o-ebl in a ZnSnO/CIGS solar cell

Parameters	1.5eV	1.7eV	1.9eV	2.1eV	2.3eV
V_{OC} (mV)	809.3	809.3	805.9	807.3	803.7
J_{SC} (mA/cm^2)	43.32	43.35	43.29	43.46	43.47
FF (%)	72.22	78.59	78.77	78.72	78.2
η (%)	25.32	27.57	27.48	27.62	27.44

D. Effect of acceptor concentration CIGS absorber layer with different energy bandgap of Cu_2O as an EBL

Fig. 5 shows the performance of electrical parameters versus acceptor doping density with different energy bandgap of Cu_2O-EBL. When the concentration of acceptor of the CIGS absorber layer is less than $1.5x10^{-16}cm^{-3}$, and the energy band gap of p-Cu_2O-EBL is less than 2.1eV, then the performance of J_{SC}, FF, and efficiency is slightly decreased.

On the other hand, if the acceptor concentration of the CIGS absorber layer is higher than $1.5x10^{-16}$ $cm^{-3}$and the energy bandgap of p- Cu_2O-EBL is higher than 2.1eV. The performance of V_{OC} and FF are increased due to a decrease of rev erse saturation current density.

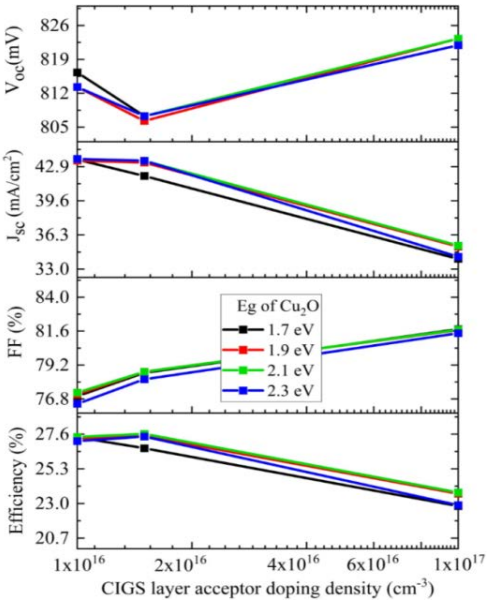

Fig. 5: Performance of electrical parameters with different acceptor doping of the CIGS absorber versus different energy bandgap of Cu_2O layer

E. The comparison between a proposed structure with the conventional one

The spectral width of 10nm with the illumination of 500nm monochromatic light and photon flux of $2.8x10^{17}cm^{-2}$ s^{-1}applied to both structures. By inserting Cu_2O -EBL in the middle of the back contact metal layer and the absorber layer, open-circuit voltage (Voc), the short circuit current density (Jsc), FF, and efficiency get improved. The Cu_2O-EBL is to minimize the photogenerated minority carrier current, which is present in the p-type region. Table IV shows that after the optimization of thickness, doping density, the energy bandgap of ZnSnO, CIGS, and Cu_2O layers, the proposed solar cell gives better results.

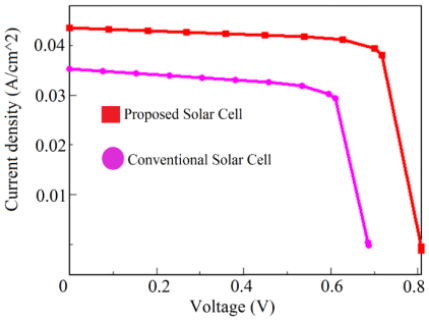

Fig. 6: Comparison of the J-V characteristics of the conventional and new structure-based solar cell

Table IV: Comparative analysis of conventional and proposed solar cell devices

Parameters	Experimental result conventional	Simulation results conventional	Proposed
V_{OC} (mV)	684	686	807.3
J_{SC} (mA/cm^2)	35.2	35.31	43.46
FF (%)	74.9	74.55	78.72
η (%)	18	18.06	27.62

CONCLUSION

In this proposed work, the 1-dimensional numerical simulation of the ZnSnO/CIGS heterojunction based solar cells applying AFORS-HET software is recommended. Here, a reference cell is discussed and simulated. The J-V curve achieves a better result in both cases (experimental as well as simulated one). P-type Cu2O used as an electron blocking layer is incorporated between the metal back-contact Mo layer, and the absorber layer CIGS provides a good outcome. By using this type of layer, cell efficiency is improved at the given different optimum values of the concentrations of doping, the energy bandgap, and the thickness for all layers. The proposed cell structure consist of ZnO:Al, ZnO, ZnSnO, CIGS and Cu2O layers with the doping concentrations of 1x1018 cm-3 , 1x1020 cm-3, 1x1019 cm-3, 1.5x1016 cm-3, 1x1016 cm-3 and thicknesses is around 50, 50, 10, 1500 and 10 nm respectively. Optimum conversion efficiency up to 27.62%, JSC = 43.46 mA/cm2, VOC = 807.3mV and FF = 78.72% is obtained for optimized cell architecture. The obtained values of the respective specifications of the proposed cell are superior to the conventional solar cell structure.

REFERENCES

1. Alqahtani, S. M., Baloch, A. A. B., Ahmed, S. S., & Alharbi, F. H. (2020). Dilute Oxygen Alloys of ZnS as a Promising Toxic-Free Buffer Layer for Cu(In,Ga)Se2 Thin-Film Solar Cells. IEEE Transactions on Electron Devices, 67(4), 1666–1673.
2. Bouabdelli, M. W., Rogti, F., Maache, M., & Rabehi, A. (2020). Performance enhancement of CIGS thin-film solar cell. Optik, 216(May).
3. Pang, J. B., Cai, Y. A., He, Q., Wang, H., Jiang, W. L., He, J. J., Yu, T., Liu, W., Zhang, Y., & Sun, Y. (2012). Preparation and Characteristics of MoSe2 Interlayer in Bifacial Cu(In,Ga)Se2 Solar Cells. Physics Procedia, 32(December), 372–378.
4. Kim, Y. J., Yoo, Y. J., Yoo, D. E., Lee, D. W., Kim, M. S., Jang, H. J., Kim, Y. C., Jang, J. H., Kang, I. S., & Song, Y. M. (2019). Enhanced Light Harvesting in Photovoltaic Devices Using an Edge-Located One-Dimensional Grating Polydimethylsiloxane Membrane [Research-article]. ACS Applied Materials and Interfaces, 11(39), 36020–36026.
5. Bahl, C. R. H., Hansen, M. F., Pedersen, T., Saadi, S., Nielsen, K. H., Lebech, B., & Mørup, S. (2006). The magnetic moment of NiO nanoparticles determined by Mössbauer spectroscopy. Journal of Physics Condensed Matter, 18(17), 4161–4175.
6. Siebentritt, S. (2004). Alternative buffers for chalcopyrite solar cells. Solar Energy, 77(6), 767–775.
7. Hamri, Y. Z., Bourezig, Y., Medles, M., Ameri, M., Toumi, K., Al-Douri, Y., Voon, C. H., & Ameri, I. (2019). Improved efficiency of Cu(In,Ga)Se2 thinfilm solar cells using a buffer layer alternative to CdS. Solar Energy, 178(November 2018), 150–156.
8. Saadat, M., Amiri, O., & Rahdar, A. (2019). Optimization of (Zn,Sn)O buffer layer in Cu(In,Ga)Se2 based solar cells. Solar Energy, 189(May), 464–470.
9. Matin, M. A., Tomal, M. U., Robin, A. M., & Amin, N. (2013). Numerical analysis of novel back surface field for high efficiency ultrathin CdTe solar cells. International Journal of Photoenergy, 2013.
10. Yang, Y., Xu, D., Wu, Q., & Diao, P. (2016). Cu2O/CuO Bilayered Composite as a High-Efficiency Photocathode for Photoelectrochemical Hydrogen Evolution Reaction. July, 1–13.
11. Boudour, S., Bouchama, I., Hadjab, M., & Laidoudi, S. (2019). Optimization of defected ZnO/Si/Cu2O heterostructure solar cell. Optical Materials, 98(August).
12. Lindahl, J., Watjen, J.T., Hultqvist, A., Ericson, T., Edoff, M., Torndahl, T., 2013a. The effect of Zn1− xSnxOy buffer layer thickness in 18.0% efficient Cd-free Cu(In,Ga)Se2solar cells. Prog. Photovolt. Res. Appl. 21 (8), 1588–1597.
13. Stangl, R., Kriegel, M., & Schmidt, M. (2006). AFORS-HET, version 2.2, a numerical computer program for simulation of heterojunction solar cells and measurements. Conference Record of the 2006 IEEE 4th World Conference on Photovoltaic Energy Conversion, WCPEC-4, 2, 1350–1353.
14. Sharbati, S., Gharibshahian, I., & Orouji, A. A. (2019). Designing of AlxGa1-xAs/CIGS tandem solar cells by an analytical model. Solar Energy, 188(February), 1–9.
15. Bouich, A., Hartiti, B., Ullah, S., Ullah, H., Touhami, M. E., Santos, D. M. F., & Mari, B. (2019). Experimental, theoretical, and numerical simulation of the performance of CuIn x Ga (1-x) S 2 -based solar cells. Optik, 183(February), 137–147.

16. Bérenguier, B., Barreau, N., Jaffre, A., Ory, D., Guillemoles, J. F., Kleider, J. P., & Lombez, L. (2019). Defects characterization in thin films photovoltaic materials by correlated high-frequency modulated and time-resolved photoluminescence: An application to Cu(In, Ga)Se2. Thin Solid Films, 669(November 2018), 520–524.
17. Tinedert, E. I., Saadoune, A., Bouchama, I., & Saeed, A. M. (2020). Numerical modelling and optimization of CdS/CdTe solar cell with incorporation of Cu2O HT-EBL layer. Optical Materials 106(April) 109970.
18. Wolfe, J. P., & Jang, J. I. (2014). The search for Bose–Einstein condensation of excitons in Cu_2O : exciton-Auger recombination versus biexciton formation. New Journal of Physics, 16(12), 123048. https://doi.org/10.1088/1367-2630/16/12/123048
19. Baig, F., Hameed, Y., Beg, S., & Marí, B. (2019). Numerical analysis of a novel CNT/Cu2O/Sb2Se3/ In2S3/ITO antimony selenide solar cell. Optik 197(February).